Hydrocracking of Polypropylene to Light Alkanes over HMFI Zeolite Catalysts under H_2

Ando, Yuriko; Miyakage, Takumi; Phuekphong, Alisa; Anzai, Akihiko; Huang, Mengwen; Fakir, Abdellah Ait El; Toyao, Takashi; Ogawa, Makoto; Kolganov, Alexander A.; Pidko, Evgeny A.

DOI
10.1002/cctc.202500512

Publication date
2025

Document Version
Final published version

Published in
ChemCatChem

ChemCatChem

Research Article
doi.org/10.1002/cctc.202500512

Chemistry Europe
European Chemical Societies Publishing

www.chemcatchem.org

Hydrocracking of Polypropylene to Light Alkanes over HMFI Zeolite Catalysts under H_2

Yuriko Ando,[a] Takumi Miyakage,[a] Alisa Phuekphong,[b] Akihiko Anzai,*[a] Mengwen Huang,[a] Abdellah Ait El Fakir,[a] Takashi Toyao,[a] Makoto Ogawa,[b] Alexander A. Kolganov,[c] Evgeny A. Pidko,[c] and Ken-ichi Shimizu*[a]

Chemical recycling of polyolefins represented by polyethylene (PE) and polypropylene (PP) via catalytic cracking has emerged as a promising strategy for converting waste plastics into valuable hydrocarbons. In this study, we investigated the selective hydrocracking of PP into light alkanes (C_1–C_5) using zeolite catalysts at 280 °C under 1 MPa H_2. An HMFI zeolite with high Al content exhibited the best catalytic performance among various zeolite catalysts tested. In situ DRIFTS comparing bare HMFI and externally-silylated HMFI suggested that the external surface Brønsted acid sites serve as the active sites for the cracking of PP. Combination of in situ DRIFTS and UV–vis spectroscopy analyses identified the formation and consumption of oligomeric species as a reaction intermediate during reaction. Density functional theory (DFT) calculations suggested that a route in which the carbocation and alkoxide intermediates generated by hydrocracking of PP undergo low-energy barrier transformations into gaseous products such as C_3 and C_4 hydrocarbons. This study advances the development of sustainable polyolefin recycling technologies.

1. Introduction

The increase in plastic waste and the environmental pollution has led to a pressing demand for sustainable recycling technologies.[1] Polyolefins, including polyethylene (PE) and polypropylene (PP) comprise a significant portion of global plastic production but are challenging to recycle because of their chemical inertness.[1]Various approaches have been proposed to address this issue such as mechanical recycle and thermal recycle.[2–4] Among the various recycling methods, chemical recycling offers a promising solution by breaking down waste plastics into their original monomers or converting them into high-value chemicals and fuels.[5–11]

Polyolefins consist of main chains formed by unreactive C(sp^3)–C(sp^3) bonds, often requiring high temperatures of 400–700 °C to cleave the bonds.[12] The initial study of noncatalytic pyrolysis at 400–550 °C yielded mainly wax-like products and when the temperature was increased to about 700 °C, gases and oils were produced.[3] In this temperature range, product selectivity remains low. Catalytic decomposition using solid acid catalysts and transition metal catalysts has been explored to address the issue. Catalytic depolymerization with solid acid catalysts such as aluminosilicate zeolites has been studied to suppress wax formation at high temperatures (e.g., above 450 °C) but the catalyst often deactivates quickly due to thermodynamically favorable coke formation and resulting in low product selectivity.[13–16] Transition metal catalysts (e.g., Pt,[6,17] Ru[5,18–20]) exhibit high activity but precious-metal-free catalysts are desirable because the high cost of precious metals imposes economic limitations on industrial applications.[13] Recently, some groups have successfully converted PE and PP to aliphatic hydrocarbons and aromatic hydrocarbons at relatively low temperatures (< 300 °C) using metal-free catalysts, zeolites such as HMFI[17,21,22] and HY.[13,23,24] Most studies have been conducted in the presence of hydrogen at high pressure. It has been suggested that the hydrogen atmosphere would contribute to improved product selectivity while suppressing coking.[25,26] However, the reaction mechanism of the light hydrocarbon production by hydrocracking of PP at relatively low temperatures (< 300 °C), including the intermediates, remains unclear, and there is a lack of spectroscopic and theoretical analysis.

In this study, we investigated the selective hydrocracking of PP to yield C_1–C_4 alkanes at 280 °C using a commercially available HMFI zeolite catalyst. Although we reported the selective catalytic cracking of PP to light olefins (C_2–C_5) at pyrolytic temperature (290 °C) without external H_2 supply over HMFI in our previous study, we only had low productivity for alkanes formation and suffered from coke formation on the catalysts.[27] The

[a] Y. Ando, T. Miyakage, Dr. A. Anzai, Dr. M. Huang, Dr. A. A. E. Fakir, Dr. T. Toyao, Prof. K.-ichi Shimizu
Institute for Catalysis, Hokkaido University, N-21, W-10, Sapporo, Hokkaido 001–0021, Japan
E-mail: anzai.akihiko@cat.hokudai.ac.jp
kshimizu@cat.hokudai.ac.jp

[b] Dr. A. Phuekphong, Prof. M. Ogawa
School of Energy Science and Engineering Vidyasirimedhi Institute of Science and Technology, 555 Moo 1 Payupnai, Wangchan, Rayong 21210, Thailand

[c] Dr. A. A. Kolganov, Prof. E. A. Pidko
Department of Chemical Engineering, Faculty of Applied Sciences, Delft University of Technology, Van der Maasweg 9, Delft, HZ 2629, The Netherlands

Yuriko Ando and Takumi Miyakage contributed equally to this work.

Supporting information for this article is available on the WWW under https://doi.org/10.1002/cctc.202500512

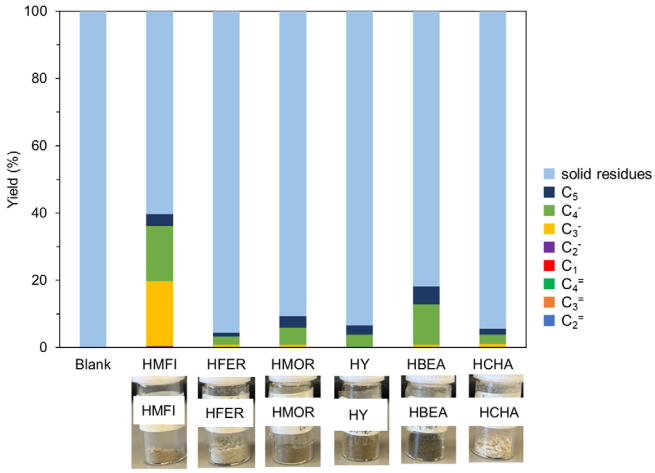

Figure 1. Product yield for PP hydrocracking by different zeolites at 280 °C (3 h, 1 MPa H_2, 0.1 g catalyst, 0.1 g PP) and photographs of catalysts after reaction. C_n^- and $C_n^=$ mean alkanes and alkenes, respectively.

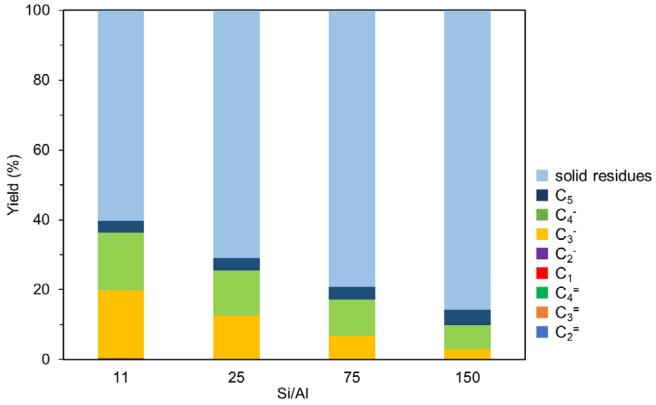

Figure 2. Product yield for PP hydrocracking by HMFI with various Si/Al ratio (280 °C, 3 h, 1 MPa H_2, 0.1 g catalyst, 0.1 g PP). C_n^- and $C_n^=$ mean alkanes and alkenes, respectively.

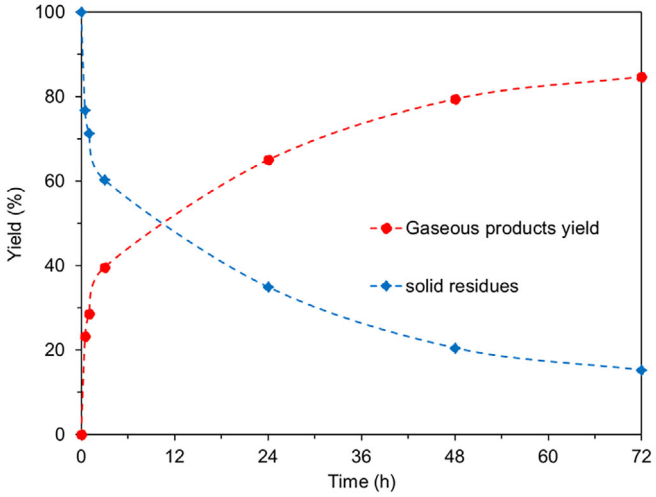

Figure 3. Time course of the yield of gaseous products and solid residues for PP hydrocracking by HMFI11 (0.1 g) at 280 °C under 1 MPa H_2.

low-temperature hydrocracking system using H_2 developed in the present study led to highly selective formation of C_3 and C_4 alkanes without significant coke formation. In situ DRIFTS and UV–vis spectroscopy analyses combining density functional theory (DFT) calculations were conducted to investigate the reaction mechanisms. The results of this study are anticipated to advance the understanding of low-temperature polyolefin cracking mechanisms and contribute to the development of environmentally sustainable plastic recycling technologies.

2. Results and Discussion

2.1. Catalyst Screening for PP Hydrocracking

Figure 1 shows the result of the PP hydrocracking by different zeolite catalysts at 280 °C for 3 h and photographs of catalysts after reaction. A blank experiment, without a catalyst, gave few products. The presence of zeolite catalysts increased the yields of hydrocarbons. Among the H^+-type zeolites screened, the total yields of gas phase hydrocarbon products depended on the type of zeolite and changed in the following order: HMFI > HBEA > HMOR > HY > HCHA > HFER, where the pore sizes are 5.8 Å for MFI, 6.5 Å for BEA, 7.0 Å for MOR, 9.0 Å for Y, 3.8 Å for CHA, and 4.8 Å for FER.[28,29] The zeolites with relatively narrow pore size (HCHA and HFER) showed relatively high yields of unreacted PP. This is because the narrow pore size limits the diffusion of PP with a large molecular weight.[30] HMFI showed the highest yield of hydrocarbons. Total yield of gaseous hydrocarbons was 39.7%. Here the yield to these products can be considered almost the same as yield of gaseous hydrocarbons because the yields of liquid hydrocarbons (C_6-C_{16}) were only trace (< 1%) (Figures S4 and S5). The major products were propane and butane and yields were 19.5% and 16.4%, respectively. Photographs of the catalysts after the reaction in Figure 1 show that after the reaction, HBEA was colored black and HY was colored dark brown. HMFI and HMOR were colored light brown. These results indicate that the PP cracking on these catalysts led to coke formation as shown in our previous study[27] and a relatively large amount of coke was deposited on HBEA and HY. Hereafter, HMFI was used as a standard catalyst for further studies.

Figure 2 compares the product yields for PP hydrocracking at 280 °C by HMFI catalysts with various Si/Al ratios. As the Si/Al ratio increased, the total yield of gaseous hydrocarbons decreased, and the yield of unreacted PP increased. The lower the Si/Al, the higher the amount of Brønsted acid sites (BAS).[31,32] This result suggests that BAS on HMFI plays an important role in this reaction. Based on the above results, we adopted HMFI11 as the standard catalyst for the optimization of the reaction conditions.

Figure 3 presents the time course of the yield of gaseous products and solid residues for PP hydrocracking on HMFI11. The yield of the solid residue was defined as the difference between the total yield and the sum of yields of C_1–C_5 gaseous products and C_6–C_{16} liquid products (see Supporting Information for Experimental details). The yield of gaseous products

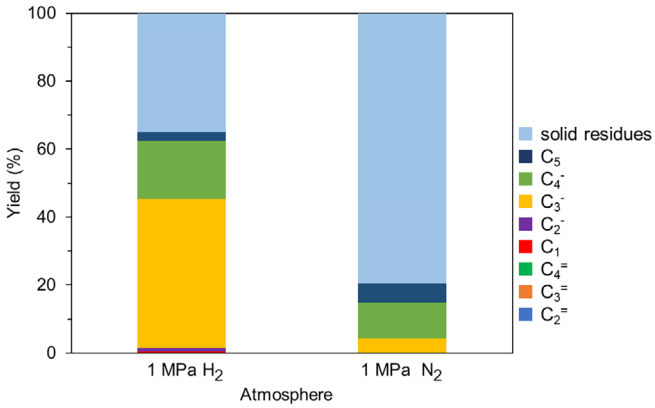

Figure 4. PP hydrocracking by HMFI11 under 1 MPa H_2 or 1 MPa N_2 (280 °C, 24 h, 0.1 g catalyst, 0.1 g PP). C_n^- and $C_n^=$ mean alkanes and alkenes, respectively.

increased with time and reached 84.7% after 72 h. As the gas yield increased, the ratio of solid residues decreased. This inverse correlation in yields suggests that the unidentified components were converted into gaseous products. To investigate the nature of these residues, we conducted solid-state ^{1}H NMR analysis (Figure S3). The spectrum obtained after heating a mixture of PP and HMFI11 to 180 °C showed typical PP-derived proton signals (0.7–1.6 ppm), suggesting the presence of unreacted PP and high molecular weight intermediates. On the other hand, these signals were significantly reduced in the residue obtained at 300 °C, which is close to the typical reaction temperature, and a new signal (2.2 ppm) that can be assigned to α-alkyl (CH_2, CH_3) groups to aromatic rings was observed.[33,34] Furthermore, the diffuse reflectance UV–vis spectrum of the solid residue shows that the absorption around 400 nm is assignable aromatic compounds such as naphthalene and anthracene, whereas the absorption around 600 nm and above 750 nm are assignable low and high molecular weight polycyclic aromatic hydrocarbons, respectively (Figure S7),[35,36] which is consistent with the results of the solid-state ^{1}H NMR analysis. These results suggest that the solid residue appears to consist of two components: (1) waxy oligomeric intermediates with 17 or more carbon atoms, which may be converted into gaseous products and (2) aromatic species, which are not converted.

To investigate the role of external H_2 in the degradation of PP on HMFI11, the depolymerization of PP was carried out under 1 MPa H_2 or N_2 atmosphere in a batch-type reactor (Figure 4). The yield of the gaseous product was 65.0% under H_2, which was about 3.2 times higher than that under N_2 (20.4%). These results suggest that the presence of H_2 promotes PP cracking.

2.2. Spectroscopic Studies on PP Depolymerization with H_2

Next, to follow the cracking process of PP under reaction conditions, in situ DRIFT spectra were recorded for the PP/HMFI11 mixture under 5 bar H_2 as the temperature was raised from 150 °C to 360 °C. Here, due to the upper pressure limit of the DRIFTS cell (5 bar), we conducted in situ DRIFTS experiments at 5 bar lower than 10 bar for reaction tests. The catalytic experiments show that product distribution had little dependence on H_2 pressure within the tested range, (Figure S1) indicating that the difference in chemical reactivity due to the pressure gap between the reaction system and in situ DRIFTS is expected to be minor. When the mixture of PP and HMFI11 was heated to 180 °C, the bands at 2958 cm^{-1} and 2873 cm^{-1}, which were assignable to asymmetric and symmetric C—H stretching of CH_3 groups, respectively[37–45] were observed. The small band at 3099 cm^{-1} is associated with the ν(C+—H) modes of allylic cations, for example, acyclic cations, alkyl-substituted cyclopentenyl cations, and also benzenium ions. (Figure 5a)[38,44–47] Upon further heating, the intensity of these bands increased rapidly, reaching a maximum at 240 °C. (Figure 5b) Considering that the melting point of PP is approximately 160 °C[49] and the background of the mixture of PP and HMFI taken at 150 °C is subtracted here, these absorption bands would be assigned to oligomeric species formed by depolymerization of PP on HMFI. At higher temperatures, the intensity of these bands decreased, indicating the cleavage of C—C bonds of PP and the formation of smaller hydrocarbons.[46,48,50] MS analysis of the outlet gas from the DRIFTS cell showed that almost no gas products were produced in the temperature range from 180 °C to 220 °C, but from around 220 °C fragments with m/z = 43, 41, 29, and 27, attributable to propane, propylene, ethane, and ethylene, respectively were mainly produced and the amount reached a maximum at 265 °C and decreased at higher temperatures (Figure 5c). Other fragments with m/z = 15, 55, 57, 69, and 71, attributable to methane, butene, butane, pentene, and pentane, respectively, were few produced. These results would suggest that BAS on HMFI11 catalyzes the dehydrogenation of C_3H_8 and the microscopic reverse reaction, hydrogenation of C_3H_6 with H_2, via a transition state such as $(C_3H_9)^+$ bound alkoxide as described by Gounder et al.[51] The negative band of 3610 cm^{-1} assigned to the O—H stretching of the bridged BAS (—Si—(OH)—Al—) was observed above 180 °C and its intensity increased up to about 240 °C. (Figure 5b) This indicated that Brønsted acidic proton was consumed. At higher temperatures, the intensity of the negative band decreased. This result possibly suggests that carbocations generated at the acid sites of HMFI11 return protons to the acid sites to generate alkenes.[49,52] The band at 1510 cm^{-1} assigned to an allylic stretching vibration ν_{as}(C=C—C+)[38,44–47] was observed above 180 °C and its intensity increased with increasing temperature up to 265 °C and then slowly decreased. Integrating these results, it could be concluded as follows: in the temperature range from 180 °C to 220 °C, PP melts first and depolymerization of PP chain into oligomers via protonation on the BAS occurs. Above 220 °C, the oligomers are protonated by BAS and produce shorter chain oligomers and finally hydrocarbon products. Some of the oligomers would form carbenium ions and be converted to polyaromatic coke species.

The BAS on the external surface of HMFI plays an important role in the cracking of PP to light hydrocarbons.[27] In this study, we also investigated the effect of external BAS (including pore mouth regions) of HMFI on hydrocracking process. The BAS on the external surface of HMFI11 was passivated by chemical liquid deposition with tetraethoxysilane (TEOS) as referred to the literature. Adsorption experiments with 2,6-di-tert-butylpyridine

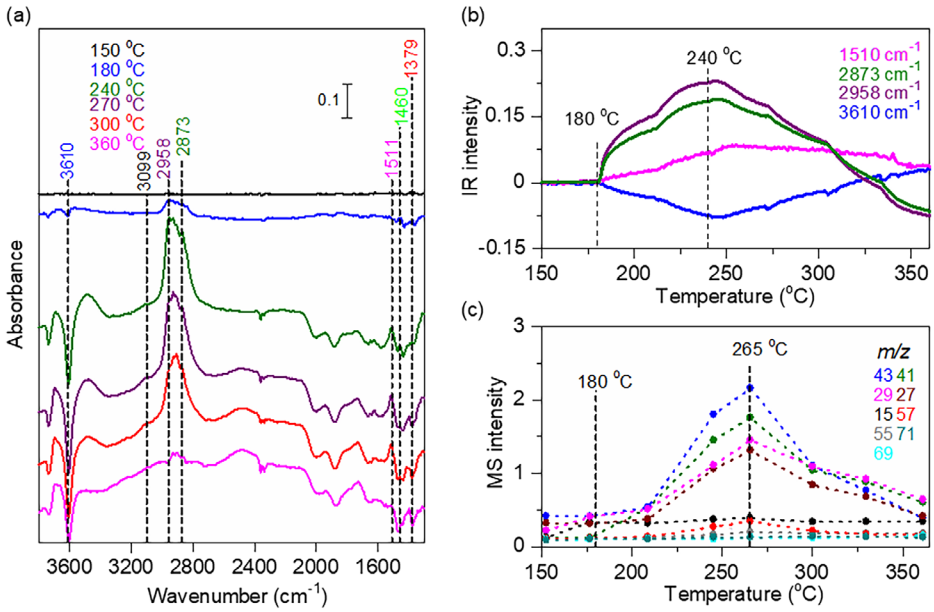

Figure 5. (a) In situ DRIFT spectra of surface species on HMFI11 during PP hydrocracking under 5 bar H_2, (b) time course of the IR intensity, and (c) MS intensity. After the measurement of the background spectrum of the sample (mixture of 2.5 mg of PP and 25 mg of HMFI11) at 150 °C, the temperature was increased from 150 °C to 360 °C during which spectra at each temperature were obtained.

(DTBPy) and pyridine (Py) performed similarly to our previous study, showed that the Brønsted acid sites on both the external and internal surfaces were passivated by TEOS treatment, but the acid sites on the external surface were passivated much more preferentially. (Figure S6)[27] The passivated HMFI11 by TEOS was named HMFI11-T. The TEOS treatment passivated the Brønsted acid sites on both the external and internal surfaces, but the acid sites on the external surfaces were more preferentially passivated.[27] Figure 6a,b show the dynamic changes of the in situ DRIFT spectra and the time course of the MS analysis of the gas products during the PP cracking under 5 bar H_2 at 300 °C over HMFI11-T and HMFI11, respectively. In the spectrum of the species on HMFI11-T, (Figure 6a) the bands at 2958 cm^{-1} and 2871 cm^{-1} assigned to the asymmetric and symmetric C—H stretching of the CH_3 group, slowly increased with time and then plateaued above 20 min. In contrast, the intensities of the bands at 2958 cm^{-1} and 2894 cm^{-1} in the spectrum of the species on HMFI11 (Figure 6b) increased sharply during the heating process from 200 °C to 300 °C and then decreased. As the bands at 2958 cm^{-1} and 2894 cm^{-1} began to decrease, the amount of gaseous hydrocarbon products, mainly fragments with m/z = 43, 41, 29, and 27 attributable to propane, propylene, ethane, and ethylene, respectively, reached a maximum. Other fragments with m/z = 15, 55, 57, 69, and 71 attributable to methane, butene, butane, pentene, and pentane, respectively, were few produced. This implies that in the early stage of the reaction, the backbone C—C bonds of oligomers cleaved mainly at the external BAS on HMFI to form smaller hydrocarbons, which leave as gaseous hydrocarbon products or are further converted to cyclic and aromatic products. In the DRIFT spectrum of HMFI11-T, the gaseous products reached a maximum after 20 min and gradually decreased. On the other hand, in the DRIFT spectrum of HMFI11, the gaseous products reached a maximum after 5 min and the reaction was terminated in about 20 min. This confirms that PP consumed relatively faster with HMFI11 than HMFI11-T, suggesting that PP cracking proceeded at a slower rate on HMFI11-T than on HMFI11. These results highlight the importance of external surface BAS in PP depolymerization.

The formation process of aromatic species over HMFI11 was investigated by in situ diffuse reflectance UV–vis spectroscopy. Figure 7 shows the UV–vis spectra and corresponding Kubelka–Munk (KM) intensities during the hydrocracking of PP over HMFI11 under 5 bar H_2 (Figure 7a) as well as the time course of online GC analysis of the UV–vis cell outlet gas. (Figure 7b) When the PP/HMFI11 mixture was heated from 29 °C to 290 °C, bands appeared at 297 nm, 431 nm, and 600 nm. The band at 297 nm assigned to a polyalkyl-substituted cyclopentenyl cation[46] increased rapidly within the first 10 min of the reaction and as soon as the band at 297 nm began to decrease, the formation rates of the gaseous hydrocarbons, mainly butane and propane measured by the online GC analysis reached a maximum. This indicates that polyalkyl-substituted cyclopentenyl cations are converted to gaseous hydrocarbon components in the early stages of the reaction (~ 20 min). In the later stage of the reaction (20 min ~), the band at 297 nm slowly decreased and the bands at 431 nm assigned to aromatic species (e.g., naphthalene and anthracene)[51,53] and 600 nm assigned to polycyclic aromatic species[51,53] that are further ring expanded from them slowly increased and plateaued. This indicates that a polyalkyl-substituted cyclopentenyl cations are converted to aromatics and polycyclic aromatic species in the late stage of the reaction (Figure 7b).

In Figure 7c,d, the difference in the coke formation process under 5 bar H_2 and He were investigated. Figure 7c shows the UV–vis spectra and corresponding KM intensities after 20 min of reaction under 5 bar He and H_2. The KM intensity at 297 nm

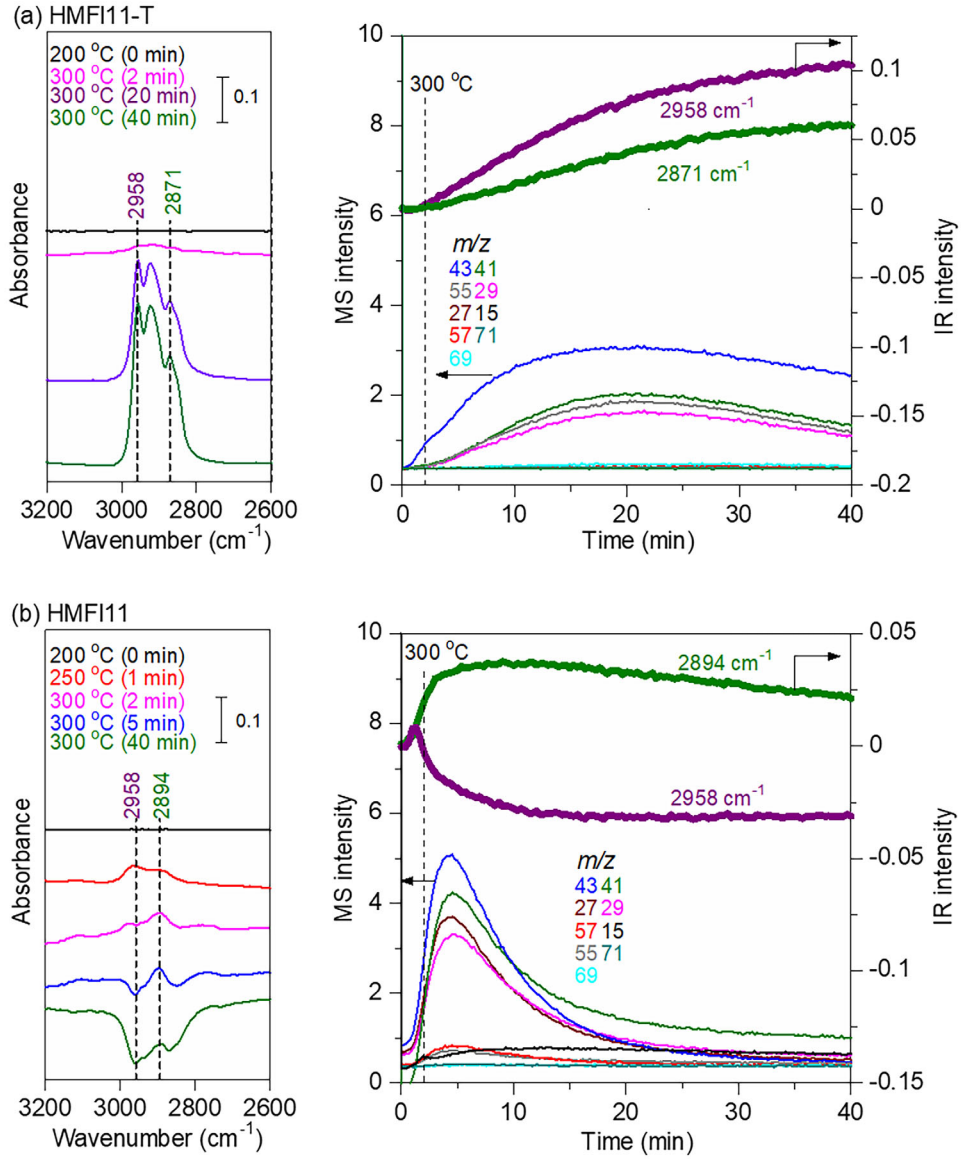

Figure 6. (a) In situ DRIFTS results during PP hydrocracking on HMFI11-T and (b) on HMFI11 under H_2: typical DRIFT spectra of adsorbed species (left) and time course of MS and IR intensity (right). After the measurement of the background spectrum of the sample (mixture of 2.5 mg PP and 25 mg zeolite) at 200 °C, the DRIFTS cell was heated to 300 °C (50 °C min^{-1} ramp rate, due to the limitations of the temperature controller attached to DRIFTS system) followed by maintaining the temperature at 300 °C.

under 5 bar H_2 was 0.85 times that under 5 bar He. This suggests that H_2 would have the effect of suppressing the initial formation of polyalkyl-substituted cyclopentenyl cations as coke intermediates. Figure 7d shows the time course of the KM intensities at 297, 431, and 600 nm under 5 bar He and H_2. Under both atmospheres, the band at 297 nm increased sharply by 10 min and then decreased with time, but the time-dependent decrease in the KM intensity at 297 nm was more pronounced under 5 bar H_2 than He. This suggests that polyalkyl-substituted cyclopentenyl cations are consumed more under 5 bar H_2 compared to He. Possible products via polyalkyl-substituted cyclopentenyl cations under H_2 include gaseous hydrocarbon products, aromatic species, and polycyclic aromatic species.[13,46] The increase in KM intensities at 431 and 600 nm with the time under 5 bar H_2 was smaller than that under He, suggesting that the conversion of polyalkyl-substituted cyclopentenyl cations to aromatic or polycyclic aromatic species would be suppressed under 5 bar H_2 compared to He. Thus, in the presence of 5 bar H_2, some of the polyalkyl-substituted cyclopentenyl cations, which can be intermediates in coke formation would be converted to gaseous hydrocarbon products and H_2 contributes to indirect coke formation suppression.

2.3. DFT Study on Mechanism of Hydrogen-Assisted Cracking of PP

The hydrogen-assisted cracking of hydrocarbons on HMFI zeolite was investigated with a focus on the role of carbocations and alkoxide intermediates in the reaction pathway. DFT cal-

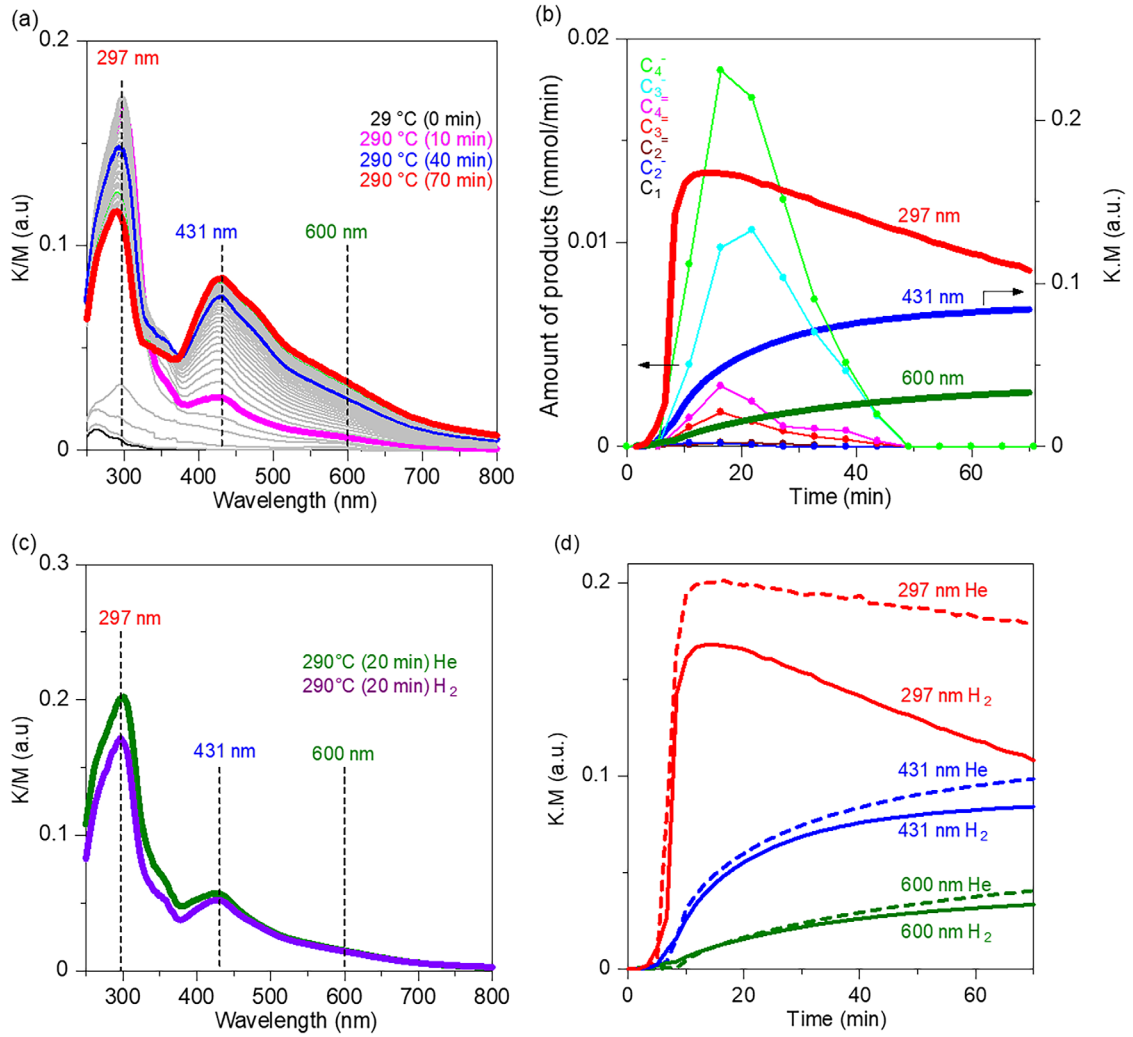

Figure 7. In situ UV–vis results during PP cracking on HMFI11 (a) typical spectra at 5 bar H_2, (b) time course of the KM (297, 431, and 600 nm) and the outlet gas (GC analysis) at 5 bar H_2. C_n^- and $C_n^=$ mean alkanes and alkenes, respectively. (c) Representative UV–vis spectra (20 min) at 5 bar He and H_2 and (d) time course of the KM intensities (297, 431, and 600 nm) at 5 bar He and H_2. After the measurement at 29 °C, the mixed-powder sample (5.7 mg PP, 57 mg HMFI11) was heated to 290 °C (20 °C min^{-1}) followed by maintaining the temperature at 290 °C.

culations were employed to explore several cracking pathways of 2,4-dimethylpentene (C_7H_{14}) as a PP oligomer model in the internal zeolite cavity.[26,27] Since the terminal C—C bonds of hydrocarbons form double bonds upon cracking,[53] an olefin was chosen as a model reactant compound in this model. Gibbs free energies were calculated by incorporating thermodynamic corrections, including zero-point energy (ZPE), thermal enthalpy contributions, and entropy effects at the reaction temperature (290 °C), into the total electronic energies obtained from DFT calculations.

Since the aforementioned experimental study demonstrated that C_3 and C_4 hydrocarbons are the primary products of PP cracking over HMFI zeolite, we investigated the reaction pathway leading to propane and isobutene from the C_7H_{14} molecule. (Figure 8)Initially, the $C_7H_{15}^+$ carbocation is generated via proton donation from the Brønsted acid site of the zeolite. Subsequently, two distinct pathways were identified: one in which the C_7 carbocation directly decomposes into propane and isobutene and another involving the formation of a propoxide intermedi-

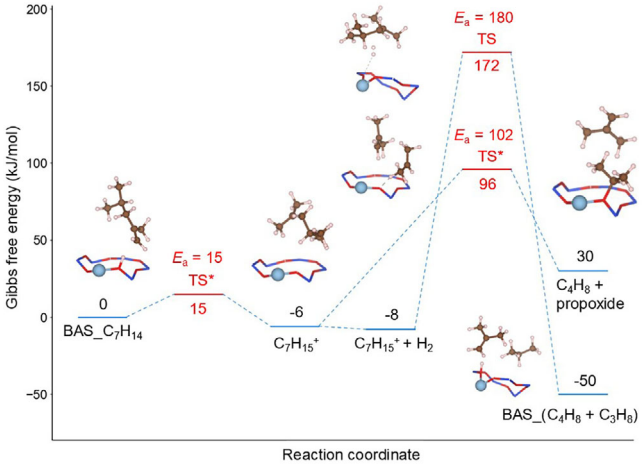

Figure 8. The reaction coordinate with the Gibbs free energy at 563 K for the two patterns of C_7H_{14} cracking on the Brønsted acid site of the HMFI zeolite, calculated using DFT. Energy values marked with * are from a previous study calculated under the same conditions.[27]

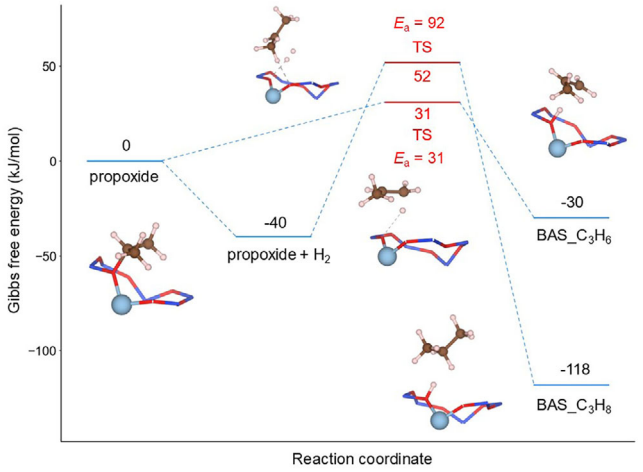

Figure 9. The reaction coordinate with the Gibbs free energy at 563 K for the propane/propylene production from the propoxide intermediate on the Brønsted acid site of the HMFI zeolite calculated by DFT.

ate prior to isobutene formation. The activation energy (E_a) of the latter pathway is 102 kJ/mol, which is significantly lower than that of the former (E_a = 180 kJ/mol) indicating that the formation of the propoxide intermediate is more favorable.

With regard to the C_3 intermediate, previous experimental studies have identified $C_3H_7^+$ as a key intermediate in the hydrogenation of propylene to produce propane.[51] Additionally, theoretical stability comparisons suggest that this species is not merely a physiosorbed carbocation but rather a propoxide species.[54] From the aforementioned calculations on the propoxide intermediate, two reaction pathways were calculated (Figure 9): one leading to propylene formation via proton donation from the Brønsted acid site of the zeolite (E_a = 31 kJ/mol) and the other involving the cleavage of an externally introduced H_2, resulting in propane formation along with the restoration of the Brønsted acid site (E_a = 92 kJ/mol). A comparison of E_a values suggests that propylene formation is more favorable. However, both E_a values are lower than that of the preceding propoxide formation step (E_a = 102 kJ/mol), suggesting the both reactions are considered feasible. These results are consistent with the experimental findings, which show that both propane and propylene are produced.

Scheme 1 shows the entire reaction pathway for the hydrogenative cracking of C_7H_{14}. First, the $C_7H_{15}^+$ carbocation is produced from the C_7H_{14} molecule via proton donation by the zeolite. Then, the carbocation undergoes cracking, yielding isobutene and propoxide intermediate. Finally, propane or propylene is produced from the propoxide intermediate (E_a = 92 or 31 kJ/mol).

Based on our experimental observations and DFT results, a plausible reaction mechanism for PP cracking under H_2 is summarized in Scheme 2 as follows: PP is first melted and cleaved to lower-molecular-weight oligomers on external BAS on the HMFI zeolite. The oligomers diffuse into the pores of the HMFI zeolite and undergo cracking on the internal Brønsted acid sites, where they are cleaved into lower molecular weight olefins such as propene and isobutene.[27] In the presence of H_2, propane is selectively produced by hydrogenative cracking of the propoxide intermediate formed on HMFI during the cracking process. Some of the produced olefins react further to form carbenium ions, which are regarded as precursors to aromatic compounds, leading to the formation of light aromatics and subsequently heavy aromatics. Some of the carbenium ions react with H_2 to produce gaseous hydrocarbons.

3. Conclusions

This study demonstrated the effective hydrocracking of polypropylene (PP) to light hydrocarbons (mainly C_3 and C_4) over HMFI below the pyrolytic temperature at 280 °C under 1 MPa H_2. Comparison of the in situ DRIFTS results for HMFI with and without TEOS treatment on the external surface indicated the Brønsted acid sites on the external surfaces of HMFI were indispensable for accelerating PP cracking and would serve as active sites for the cracking of PP into short-chain (oligomeric) hydrocarbon species that lead to formation of final gaseous hydrocarbon products. The results of in situ DRIFTS and UV–vis experiments suggested that the effect of external H_2 was to suppress the formation of coke intermediates such as alkyl-substituted cyclopentenyl cation. Adopting 2,4-dimethylheptene as a model oligomeric species, possible reaction pathways were calculated using DFT. The protonation of 2,4-dimethylheptene by a Brønsted acid site yields $C_7H_{15}^+$ carbocation intermediate, which reacts with H_2 to produce propane and isobutene.

4. Experimental Section

4.1. Materials

Polypropylene (PP, isotactic, average M_w ~12000) were purchased from Sigma–Aldrich Co. Ltd. NH_4–MFI (Si/Al = 11.15), NH_4–Chabazite (Si/Al = 11.15), NH_4–Ferrierite (Si/Al = 9), NH_4–Beta (Si/Al = 8.76), H–Mordenite (Si/Al = 9.1), H–Y type zeolite (Si/Al = 5.3), and H-MFI (Si/Al = 25,75150) were provided by Tosoh corporation Co. Ltd.

4.2. Catalyst Preparation

NH_4^+-type zeolites (NH_4–MFI, NH_4–Chabazite, NH_4–Ferrierite, and NH_4–BEA) were converted to H^+-type by calcination at 500 °C for 1 h under an air flow using heating rate of 10 °C/min. These catalysts were denoted as HMFI, HCHA, HFER, and HBEA, respectively. H^+-type zeolites (H–Mordenite, H–Y type zeolite, H-MFI (Si/Al = 25,75150)) were used without further treatment. These catalysts were denoted as HMOR and HY, respectively. If a number appears next to the name of the catalyst, it indicates Si/Al ratio. For example, HMFI with Si/Al ratio of 11 is denoted HMFI11. Tetraethoxysilane (TEOS)-treated HMFI11 (HMFI11-T) was prepared by refluxing a mixture of HMFI11 (2 g, dried at 100 °C) and TEOS (0.24 mmol) in *n*-hexane (50 mL) for 1 h, followed by filtering and washing with toluene and acetone, drying at 100 °C for 1 h, and calcining at 600 °C for 1 h. Next, TEOS (0.24 mmol) was added to this catalyst in *n*-hexane (50 mL); the solution was refluxed, washed, and dried as before.[27]

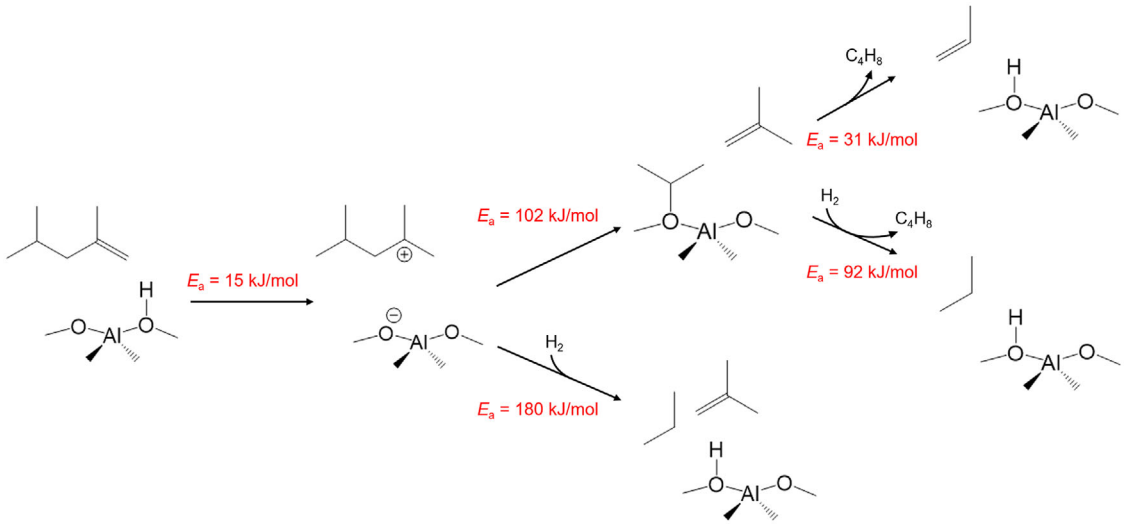

Scheme 1. The entire reaction pathway for the hydrogenative cracking of C_7H_{14} on the Brønsted acid site of the HMFI zeolite calculated by DFT.

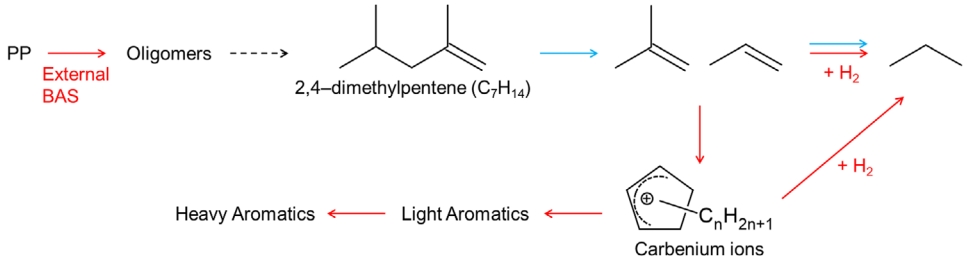

Scheme 2. Proposed mechanism for the catalytic cracking of PP over HMFI zeolite under H_2. The red and light blue arrows represent experimentally and computationally confirmed pathways, respectively, in the present study.

4.3. Hydrocracking of Polypropylene

Hydrocracking reactions of PP were carried out in a stainless-steel batch reactor (Taiatsu Techno Corp.,10 mL) without solvent. Catalyst, PP (0.1 g respectively) and glass-coated magnetic stirrer bar were added in a glass tube 6.5 cm^3, which was then inserted into the stainless-steel reactor. A catalyst: polymer ratio of 1:1 was selected to reduce solid residues and obtain higher gaseous product yields.[18] The reactor was sealed with Teflon gasket and tightened and was pressurized with H_2 (typically 1 MPa H_2) gas for ten times prior to the reaction to eliminate air from the reactor. The reactor was placed in a heating block at the desired temperature (typically 280 °C) and stirred (4000 rpm) for a given reaction time. After the reaction, followed by cooling the reactor, the gaseous products in head space of reactor were transferred into an aluminum gas sampling bag. Chloroform (0.062 mmol (5 µL)) as an internal standard was introduced into the gas sampling bag (1 L). Then, the gas products were analyzed and quantified by gas chromatography-flame ionization detector (GC-2014 FID, Shimadzu) equipped with Porapak Q column. Liquid products were extracted by washing with 2 mL of acetone (Figures S4 and S5).[55–57] The liquid part was separated from solid residue by centrifugation. Decane was introduced to liquid products as an internal standard. Then, the liquid product was analyzed by gas chromatography-flame ionization detector (GC-2014 FID, Shimazu) equipped with UA-1 column. The solids after reaction were weighed and the mass of the catalyst was subtracted to record the reaction conversion.

4.4. Catalyst Characterization

In situ diffuse reflectance infrared Fourier transform (DRIFT) spectra were recorded on a JASCO FT/IR-4600 instrument equipped with a Mercury–Cadmium–Telluride (MCT) detector. A mixture of PP and catalyst powder was packed into the sample holder in a DRIFTS cell (DR-650 Ci) equipped with a ZnSe window. The catalyst to polymer ratio was set to 10:1, a ratio that provides stable baseline behavior, in order to suppress baseline drift due to polymer melting and volume shrinkage. The inlet of the cell was connected to a flow reaction system (total flow: 30 mL min^{-1}). The spectra were measured by accumulating 20 scans at a resolution of 8 cm^{-1}, 0.5 MPa, and temperature range of 150–360 °C. The reference spectrum in He flow (20 scans) taken at the measurement temperature was subtracted from each spectrum. Outlet gas was analyzed using mass spectrometer (BELMass, MicrotracBEL Corp).

In situ diffuse reflectance UV–vis experiments under catalytic conditions were carried out by a JASCO V-750 UV–vis spectrometer of PP and catalyst powder sample (50 mg) mixed in specified proportions was placed in the in situ cell (JASCO HISV-728) with a quartz window. The inlet of the cell was connected to the gas flow system connected to a flow reaction system (total flow: 30 mL min^{-1}). The background spectrum was obtained using $BaSO_4$. Reflectance data were converted to pseudo-absorbance using the Kubelka–Munk (KM) function. For selected in situ experiments, the outlet gas of the in situ cell was connected online gas chromatograph (GC) with a TCD detector (Agilent 990 Micro GC).

4.5. Computational Details

All calculations were carried out using periodic density functional theory (DFT) simulations performed with the CP2K 2023.2 software package.[58] The structure of the MFI zeolite was obtained from the International Zeolite Association database.[59] The parameters for the MFI structure were set to $a = 20.090$ Å, $b = 19.738$ Å, and $c = 13.142$ Å. The T12 silicon of the MFI model was chosen for replacement with an Al atom based on its stability.[60] The generalized gradient approximation (GGA) with the Perdew–Burke–Ernzerhof (PBE) functional was used to describe the exchange-correlation energy, including empirical dispersion corrections by Grimme's D3 scheme with Becke–Johnson damping.[61–63] The periodic Poisson solver was utilized in combination with Goedecker–Teter–Hutter (GTH) pseudopotentials.[64,65] A cutoff of 450 Ry and a relative cutoff of 50 Ry were applied for the plane-wave basis set. A DZVP-MOLOPT-SR-GTH basis set was used. The orbital transformation (OT) method with direct inversion in the iterative subspace (DIIS) minimizer and full single-inverse preconditioner was employed to accelerate self-consistent field (SCF) convergence.[66] The structural optimization was performed with the Broyden–Fletcher–Goldfarb–Shanno (BFGS) optimizer.[67–70] The SCF convergence criterion was set to 1.0×10^{-6} Hartrees with a maximum of 300 SCF iterations.

The climbing-image nudged-elastic-band (CI-NEB) method was employed to locate the transition state.[71] The climbing process was initiated after five initial NEB steps. The number of replicas was set to 8. After the CI-NEB, the structural optimization for locating the transition state was performed with the dimer method[72,73] and the conjugate gradient (CG) optimizer.[74] The maximum number of steepest descent steps for the CG optimizer was set to zero and a two-point line-search method was employed with a maximum allowed step of 0.01 Bohr.

Vibrational analysis was performed using finite differences method with a displacement parameter (DX) of 0.01 Å and fully periodic boundary conditions. The calculations considered only the vibrational frequencies of the extra-framework atoms, whereas all other atoms were fixed. Details of the Gibbs free energy calculations are provided in the Supporting Information.

Supporting Information

The Supporting Information is available free of charge at https://pubs.acs.org/doi/XXXXX. Detail information about DFT calculations.

Author Contributions

Akihiko Anzai and Ken-ichi Shimizu designed the study. Yuriko Ando conducted the catalytic reactions and data analysis with the help of Alisa Phuekphong, Mengwen Huang, and Makoto Ogawa. Yuriko Ando, Abdellah Ait El Fakir, and Akihiko Anzai performed mechanistic studies using in situ spectroscopies. Takumi Miyakage performed DFT calculations with the help of Alexander A. Kolganov, Evgeny A. Pidko, and Takashi Toyao. The manuscript was written by Yuriko Ando, Takumi Miyakage, Akihiko Anzai, Ken-ichi Shimizu, and Takashi Toyao with input from all authors. Finally, all authors approved the final version.

Acknowledgments

This study was financially supported by KAKENHI (Grant Nos. 21H04626, 23KF0129, 23K26690, and 23K20034) from Japan Society for the Promotion of Science (JSPS). Abdellah Ait El Fakir acknowledges a JSPS Postdoctoral Fellowship (P23351). This study was also supported by the Joint Usage/Research Center for Catalysis. A portion of the calculations was performed on supercomputers at ACCMS (Kyoto University). Alexander A. Kolganov and Evgeny A. Pidko thank the NWO Domein Exacte en Natuurwetenschappen for the use of the Dutch national supercomputer, Snellius.

Conflict of Interests

The authors declare no conflict of interest.

Data Availability Statement

The data that support the findings of this study are available from the corresponding author upon reasonable request.

Keywords: Hydrocracking · In situ spectroscopy · Mild conditions · Polyolefin upcycling · Zeolite

[1] R. Geyer, J. R. Jambeck, K. L. Law, *Sci. Adv.* **2017**, *3*, e1700782 https://doi.org/10.1126/sciadv.1700782.
[2] I. Vollmer, M. J. F. Jenks, M. C. P. Roelands, R. J. White, T. van Harmelen, P. de Wild, G. P. van der Laan, F. Meirer, J. T. F. Keurentjes, B. M. Weckhuysen, *Angew. Chem., Int. Ed.* **2020**, *59*, 15402–15423.
[3] W. Kaminsky, *Fuel Commun.* **2021**, *8*, 100023.
[4] N. M. Wang, G. Strong, V. Dasilva, L. Gao, R. Huacuja, I. A. Konstantinov, M. S. Rosen, A. J. Nett, S. Ewart, R. Geyer, S. L. Scott, D. Guironnet, *J. Am. Chem. Soc.* **2022**, *144*, 18526–18531.
[5] Q. Kang, M. Chu, P. Xu, X. Wang, S. Wang, M. Cao, O. Ivasenko, T. K. Sham, Q. Zhang, Q. Sun, J. Chen, *Angew. Chem., Int. Ed.* **2023**, *62*, e202313174 https://doi.org/10.1002/anie.202313174.
[6] G. Celik, R. M. Kennedy, R. A. Hackler, M. Ferrandon, A. Tennakoon, S. Patnaik, A. M. Lapointe, S. C. Ammal, A. Heyden, F. A. Perras, M. Pruski, S. L. Scott, K. R. Poeppelmeier, A. D. Sadow, M. Delferro, *ACS Cent. Sci.* **2019**, *5*, 1795–1803.
[7] J. Su, G. Xu, B. Dong, R. Yang, H. Sun, Q. Wang, *Polym. Chem.* **2022**, *13*, 5897–5904.
[8] Z. Xu, N. E. Munyaneza, Q. Zhang, M. Sun, C. Posada, P. Venturo, N. A. Rorrer, J. Miscall, B. G. Sumpter, G. Liu, *Science* **2023**, *381*, 666–671.
[9] B. A. Abel, R. L. Snyder, G. W. Coates, *Science 1979* **2021**, *373*, 783–789.
[10] J. Huang, A. Veksha, W. P. Chan, A. Giannis, G. Lisak, *Renewable Sustainable Energy Rev.* **2022**, *154*, 111866.
[11] L. D. Ellis, N. A. Rorrer, K. P. Sullivan, M. Otto, J. E. McGeehan, Y. Román-Leshkov, N. Wierckx, G. T. Beckham, *Nat. Catal.* **2021**, *4*, 539–556.
[12] R. E. Harmon, G. SriBala, L. J. Broadbelt, A. K. Burnham, *Energy Fuels* **2021**, *35*, 6765–6775.
[13] Z. Chen, X. Zhang, F. Yang, H. Peng, X. Zhang, S. Zhu, L. Che, *Appl Catal A Gen* **2021**, *609*, 117873 https://doi.org/10.1016/j.apcata.2020.117873.
[14] A. Feller, J. O. Barth, A. Guzman, I. Zuazo, J. A. Lercher, *J. Catal.* **2003**, *220*.
[15] B. Thangaraj, Y. K. Lee, *Fuel* **2025**, *380*, 133220.
[16] Z. Dong, W. Chen, K. Xu, Y. Liu, J. Wu, F. Zhang, *ACS Catal.* **2022**, *12*, 14882–14901.
[17] J. Z. Tan, C. W. Hullfish, Y. Zheng, B. E. Koel, M. L. Sarazen, *Appl. Catal. B* **2023**, *338*, 123028 https://doi.org/10.1016/j.apcatb.2023.123028.

[18] J. E. Rorrer, G. T. Beckham, Y. Román-Leshkov, *JACS Au* **2021**, *1*, 8–12.
[19] M. Tamura, S. Miyaoka, Y. Nakaji, M. Tanji, S. Kumagai, Y. Nakagawa, T. Yoshioka, K. Tomishige, *Appl. Catal. B* **2022**, *318*, 121870 https://doi.org/10.1016/j.apcatb.2022.121870.
[20] C. Wang, T. Xie, P. A. Kots, B. C. Vance, K. Yu, P. Kumar, J. Fu, S. Liu, G. Tsilomelekis, E. A. Stach, W. Zheng, D. G. Vlachos, *JACS Au* **2021**, *1*, 1422–1434.
[21] K. A. Tarach, M. Akouche, K. Pyra, V. Valtchev, G. Jajko, J. P. Gilson, K. Góra-Marek, *Appl. Catal. B* **2023**, *334*, 122871.
[22] Z. Zhang, H. Chen, G. Li, W. Hu, B. Niu, D. Long, Y. Zhang, *ACS Catal.* **2024**, *14*, 2552–2561.
[23] L. C. Lerici, M. S. Renzini, L. B. Pierella, *Procedia Mater. Sci.* **2015**, *8*, 297–303.
[24] S. Liu, P. A. Kots, B. C. Vance, A. Danielson, D. G. Vlachos, *Sci. Adv* **2021**, *7*, eabf8283.
[25] J. H. Miller, A. K. Starace, D. A. Ruddy, *ChemSusChem* **2022**, *15*, e202200535 https://doi.org/10.1002/cssc.202200535.
[26] J. Duan, W. Chen, C. Wang, L. Wang, Z. Liu, X. Yi, W. Fang, H. Wang, H. Wei, S. Xu, Y. Yang, Q. Yang, Z. Bao, Z. Zhang, Q. Ren, H. Zhou, X. Qin, A. Zheng, F. S. Xiao, *J. Am. Chem. Soc.* **2022**, *144*, 14269–14277.
[27] Y. Ando, T. Miyakage, A. Anzai, M. Huang, A. Ait El Fakir, T. Toyao, Y. Nakasaka, A. Phuekphong, M. Ogawa, A. A. Kolganov, E. A. Pidko, K. Shimizu, *J. Phys. Chem. C* **2025**, *129*, 1678–1691.
[28] TOSOH, Tosoh's zeolite grades, https://www.tosoheurope.com/File%20Library/TSEB/GlobalNav/OUR%20PRODUCTS/Zeolite/Tosoh-Zeolite-Grades_English_2023.pdf (accessed: March **2025**).
[29] C. Baerlocher, L. B. McCusker, R. Hanson, Database of Zeolite Structures, https://www.iza-structure.org/databases/, (accessed: March **2025**).
[30] O. Rogala, K. A. Tarach, L. Lakiss, A. Kordek, V. Valtchev, J.-P. Gilson, K. Góra-Marek, *Appl. Catal. B: Environ. and Energy* **2024**, *365*, 124893.
[31] R. Wei, H. Yang, J. A. Scott, K. F. Aguey-Zinsou, D. Zhang, *Mater. Today Chem.* **2018**, *8*, 1–12 https://doi.org/10.1016/j.mtchem.2018.01.002.
[32] A. Korde, B. Min, Q. Almas, Y. Chiang, S. Nair, C. W. Jones, *ChemCatChem* **2019**, *11*, 4548-4557.
[33] R. Meusinger, *Fuel* **1996**, *75*, 1235–1243.
[34] V. Bansal, S. Vatsala, G. S. Kapur, B. Basu, A. S. Sarpal, *Energy Fuels* **2004**, *18*, 1505–1511.
[35] D. Fu, O. van der Heijden, K. Stanciakova, J. E. Schmidt, B. M. Weckhuysen, *Angew. Chem., Int. Ed.* **2020**, *59*, 15502–15506, https://doi.org/10.1002/anie.201916596.
[36] D. Mores, J. Kornatowski, U. Olsbye, B. M. Weckhuysen, *Chem. – A Euro. J.* **2011**, *17*, 2874–2884, https://doi.org/10.1002/chem.201002624.
[37] J. Coates, Interpretation of infrared spectra, a practical approach, Encyclopedia of Analytical Chemistry **2000**, *12*, 10815–10837.
[38] L. Maggiulli, V. L. Sushkevich, O. Kröcher, J. A. van Bokhoven, D. Ferri, *ACS Catal.* **2024**, *14*, 11477–11489.
[39] I. Vollmer, M. J. F. Jenks, S. Rejman, F. Meirer, A. Gurinov, M. Baldus, B. M. Weckhuysen, *Catal. Sci. Technol.* **2024**, *14*, 894–902.
[40] P. Castaño, G. Elordi, M. Olazar, A. T. Aguayo, B. Pawelec, J. Bilbao, *Appl. Catal. B* **2011**, *104*, 91–100.
[41] K. Pyra, K. A. Tarach, D. Majda, K. Góra-Marek, *Catal. Sci. Technol.* **2019**, *9*, 1794–1801.
[42] V. Kazansky, I. Subbotina, F. Jentoft, *J. Catal.* **2006**, *240*, 66–72.
[43] S. Bodoardo, R. Chiappetta, F. Fajula, E. Garrone, *Micropor. Mater.* **1995**, *3*, 613–622.
[44] I. B. Minova, S. K. Matam, A. Greenaway, C. R. A. Catlow, M. D. Frogley, G. Cinque, P. A. Wright, R. F. Howe, *Phys. Chem. Chem. Phys.* **2020**, *22*, 18849–18859.
[45] M. J. Wulfers, F. C. Jentoft, *J. Catal.* **2013**, *307*, 204–213.
[46] E. D. Hernandez, F. C. Jentoft, *ACS Catal.* **2020**, *10*, 5764–5782.
[47] I. Kiricsi, H. Förster, G. Tasi, J. B. Nagy, *Chem. Rev.* **1999**, *99*, 2085–2114.
[48] N. Pasquini, *Polypropylene Handbook*, Hanser Publishers, Munich **2005**.
[49] E. T. C. Vogt, B. M. Weckhuysen, *Chem. Soc. Rev.* **2015**, *44*, 7342–7370.
[50] V. B. Kazansky, I. R. Subbotina, F. Jentoft, *J. Catal.* **2006**, *240*, 66–72.
[51] R. Gounder, E. Iglesia, *J. Catal.* **2011**, *277*, 36–45.
[52] R. Zhao, G. L. Haller, J. A. Lercher, *Microporous Mesoporous Mater.* **2023**, *358*, 112390.
[53] J. Rey, C. Bignaud, P. Raybaud, T. Bučko, C. Chizallet, *Angew. Chem., Int. Ed.* **2020**, *59*, 18938–18942.
[54] A. Bhan, Y. V. Joshi, W. N. Delgass, K. T. Thomson, *J. Phys. Chem. B* **2003**, *107*, 10476–10487.
[55] J. E. Rorrer, C. Troyano-Valls, G. T. Beckham, Y. Román-Leshkov, *ACS Sustain. Chem. Eng.* **2021**, *9*, 11661–11666 https://doi.org/10.1021/acssuschemeng.1c03786.
[56] A. De Stefanis, P. Cafarelli, F. Gallese, E. Borsella, A. Nana, G. Perez, *J. Anal. Appl. Pyrolysis* **2013**, *104*, 479-484.
[57] W. C. Huang, M. S. Huang, C. F. Huang, C. C. Chen, K. L. Ou, *Fuel* **2010**, *89*, 2305–2316 https://doi.org/10.1016/j.fuel.2010.04.013.
[58] T. D. Kühne, M. Iannuzzi, M. Del Ben, V. V. Rybkin, P. Seewald, F. Stein, T. Laino, R. Z. Khaliullin, O. Schütt, F. Schiffmann, D. Golze, J. Wilhelm, S. Chulkov, M. H. Bani-Hashemian, V. Weber, U. Borštnik, M. Taillefumier, A. S. Jakobovits, A. Lazzaro, H. Pabst, T. Müller, R. Schade, M. Guidon, S. Andermatt, N. Holmberg, G. K. Schenter, A. Hehn, A. Bussy, F. Belleflamme, G. Tabacchi, A. Glöß, M. Lass, I. Bethune, C. J. Mundy, C. Plessl, M. Watkins, J. VandeVondele, M. Krack, J. Hutter, *J. Chem. Phys.* **2020**, *152*, 194103 https://doi.org/10.1063/5.0007045.
[59] Ch. Baerlocher, L. B. McCusker, R. Hanson, Database of Zeolite Structures, https://www.iza-structure.org/databases/, (accessed: March **2025**).
[60] A. Ghorbanpour, J. D. Rimer, L. C. Grabow, *Catal. Commun.* **2014**, *52*, 98–102 https://doi.org/10.1016/j.catcom.2014.04.005.
[61] J. P. Perdew, K. Burke, M. Ernzerhof, *Phys. Rev. Lett.* **1996**, *77*, 3865 https://doi.org/10.1103/PhysRevLett.77.3865.
[62] S. Grimme, J. Antony, S. Ehrlich, H. Krieg, *J. Chem. Phys.* **2010**, *132*, 154104, https://doi.org/10.1063/1.3382344.
[63] S. Grimme, S. Ehrlich, L. Goerigk, *J. Comput. Chem.* **2011**, *32*, 1456-1465 https://doi.org/10.1002/jcc.21759.
[64] S. Goedecker, M. Teter, *Phys. Rev. B Condens. Matter. Mater. Phys.* **1996**, *54*, 1703 https://doi.org/10.1103/PhysRevB.54.1703.
[65] C. Hartwigsen, S. Goedecker, J. Hutter, *Phys. Rev. B Condens. Matter. Mater. Phys.* **1998**, *58*, 3641 https://doi.org/10.1103/PhysRevB.58.3641.
[66] J. VandeVondele, J. Hutter, *J. Chem. Phys.* **2003**, *118*,4365–4369.
[67] C. G. Broyden, *IMA J. Appl. Math.* **1970**, *6*, 76–90 https://doi.org/10.1093/imamat/6.1.76.
[68] R. Fletcher, *Comput. J.* **1970**, *13*, 317–322 https://doi.org/10.1093/comjnl/13.3.317.
[69] D. Goldfarb, *Math Comput.* **1970**, *24*, 23–26 https://doi.org/10.1090/s0025-5718-1970-0258249-6.
[70] D. F. Shanno, *Math Comput.* **1970**, *24*, 647–656 https://doi.org/10.1090/s0025-5718-1970-0274029-x.
[71] G. Henkelman, B. P. Uberuaga, H. Jónsson, *J. Chem. Phys.* **2000**, *113*, 9901–9904 https://doi.org/10.1063/1.1329672.
[72] J. Kästner, P. Sherwood, *J. Chem. Phys.* **2008**, *128*, 014106, https://doi.org/10.1063/1.2815812.
[73] G. Henkelman, H. Jónsson, *J. Chem. Phys.* **2000**, *113*, 9978–9985 https://doi.org/10.1063/1.1323224.
[74] H. Chaffey-Millar, A. Nikodem, A. V. Matveev, S. Krüger, N. Rösch, *J. Chem. Theory Comput.* **2012**, *8*,777-786.

Manuscript received: March 22, 2025
Revised manuscript received: May 19, 2025
Accepted manuscript online: May 23, 2025
Version of record online: ■■, ■■